Received: 17 March 2019 | Revised: 20 August 2019 | Accepted: 22 August 2019

DOI: 10.1111/ejn.14560

RESEARCH REPORT

EJN European Journal of Neuroscience FENS WILEY

Nasal respiration entrains neocortical long-range gamma coherence during wakefulness

Matías Cavelli[1] | **Santiago Castro-Zaballa**[1] | **Joaquín Gonzalez**[1] | **Daniel Rojas-Líbano**[2] | **Nicolas Rubido**[3] | **Noelia Velásquez**[1] | **Pablo Torterolo**[1]

[1]Laboratorio de Neurobiología del Sueño, Departamento de Fisiología, Facultad de Medicina, Universidad de la República, Montevideo, Uruguay

[2]Laboratorio de Neurociencia Cognitiva y Social, Facultad de Psicología, Universidad Diego Portales, Santiago, Chile

[3]Facultad de Ciencias, Instituto de Física, Universidad de la República, Montevideo, Uruguay

Correspondence
Pablo Torterolo, Laboratorio de Neurobiología del Sueño, Departamento de Fisiología, Facultad de Medicina, Universidad de la República, Montevideo, Uruguay.
Email: ptortero@fmed.edu.uy

Funding information
"Comision Sectorial de Investigacion Cientifica – CSIC"; "Comisión de Apoyo a Postgrados - CAP"; Proyecto Fondecyt, Grant/Award Number: 3120185; "Ageancia Nacional de Investigación e Innovación, ANII"; "Programa de Desarrollo de Ciencias Basicas - PEDECIBA"; "Agencia Nacional de Investigación en Innovación - ANII"

The peer review history for this article is available at https://publons.com/publon/10.1111/EJN.14560

Abstract

Recent studies have shown that slow cortical potentials in archi-, paleo- and neocortex can phase-lock with nasal respiration. In some of these areas, gamma activity (γ: 30–100 Hz) is also coupled to the animal's respiration. It has been hypothesized that these functional relationships play a role in coordinating distributed neural activity. In a similar way, inter-cortical interactions at γ frequency have also been associated as a binding mechanism by which the brain generates temporary opportunities necessary for implementing cognitive functions. The aim of the present study is to explore whether nasal respiration entrains inter-cortical functional interactions at γ frequency during both wakefulness and sleep. Six adult cats chronically prepared for electrographic recordings were employed in this study. Our results show that during wakefulness, slow cortical respiratory potentials are present in the olfactory bulb and several areas of the neocortex. We also found that these areas exhibit cross-frequency coupling between respiratory phase and γ oscillation amplitude. We demonstrate that respiratory phase modulates the inter-cortical gamma coherence between neocortical electrode pairs. On the contrary, slow respiratory oscillation and γ cortical oscillatory entrainments disappear during non-rapid eye movement and rapid eye movement sleep. These results suggest that a single unified phenomenon involves cross-frequency coupling and long-range γ coherence across the neocortex. This fact could be related to the temporal binding process necessary for cognitive functions during wakefulness.

KEYWORDS
binding, breathing, modulation, sleep and cataplexy, synchronization

Abbreviations: ACF, autocorrelation function; ANOVA, analysis of variance; CA, cataplexy; CCF, cross-correlation function; CFC, cross-frequency coupling; CRP, cortical respiratory potential; ECoG, electrocorticogram; EEG, electroencephalogram; EMG, electromyogram; i.p., intraperitoneal; LFP, local field potential; LGN, lateral geniculate nucleus; L, left; M1, primary motor cortex; MI, modulation index; NPO, nucleus pontis oralis; NREM, non-REM sleep; OB, olfactory bulb; OSN, olfactory sensory neurons; PAC, phase–amplitude coupling; Pf, prefrontal cortex; PGO waves, ponto–geniculo–occipital waves; PLV, phase locking value; REMc, REM carbachol; REM, rapid eye movement; rmANOVA, repeated-measures ANOVA; RMS, root mean square; s.c., subcutaneous; S1, primary somatosensory cortex; SD, standard deviation; V1, primary visual cortex; V2, secondary visual cortex; W, wakefulness; **γ**, gamma.

Edited by László Acsády.

1 | INTRODUCTION

The brain is a complex system in which parallel processing coexists with serial operations within highly inter-connected networks but without a single coordinating center. This organ integrates neural events that occur at different times and locations into a unified perceptual experience. Understanding the mechanisms responsible for this integration is a crucial challenge for cognitive neuroscience (Cavelli et al., 2017; Fries, 2009; Singer, 1999; Von der Malsburg, 1995).

Neural synchronization at gamma frequency band (γ: 30–100 Hz) is considered a binding mechanism utilized by the brain to generate transient opportunities for communication and integration of the distributed neural activity necessary for cognitive functions (Buzsáki & Draguhn, 2004; Engel, Fries, & Singer, 2001; Fries, 2009; Gray, König, Engel, & Singer, 1989; Salinas & Sejnowski, 2001; Singer, 1999; Varela, Lachaux, Rodriguez, & Martinerie, 2001). For example, cortical γ power increases during active behavioral states as well as during the performance of cognitive tasks (Buzsáki & Schomburg, 2015; Castro-Zaballa, Falconi, Chase, & Torterolo, 2013; Cavelli et al., 2017; Manabe & Mori, 2013; Rojas-Líbano, Frederick, Egaña, & Kay, 2014; Varela et al., 2001). Besides, γ synchronization between distant areas of the brain (γ coherence) also increases during several cognitive functions in both animals and humans (Bressler, Coppola, & Nakamura, 1993; Castro-Zaballa et al., 2013; Cavelli et al., 2017; Rodriguez et al., 1999; Varela et al., 2001). γ Coherence has been considered a neural correlate of conscious perception (Joliot, Ribary, & Llinás, 1994; Melloni et al., 2007; Rodriguez et al., 1999; Varela et al., 2001); it decreases during sleep (Castro-Zaballa et al., 2013, 2014; Cavelli et al., 2015, 2017) and is absent during narcosis (unconsciousness) induced by general anesthetics (John, 2002; Mashour, 2006; Pal, Silverstein, Lee, & Mashour, 2016). Recently, it was shown that slow oscillations such as theta rhythm of the hippocampal networks (Cavelli et al., 2018; Scheffzük et al., 2011; Tort, Scheffer-Teixeira, Souza, Draguhn, & Brankačk, 2013; Tort et al., 2008; Zhong et al., 2017), cortical potentials caused by the rhythmic movement of the eyes (Ito, Maldonado, & Grün, 2013; Lowet et al., 2018) and respiration (Ito et al., 2014; Tort, Brankačk, & Draguhn, 2018a; Zhong et al., 2017) modulate γ activity.

Adrian's report was the first description of nasal respiration driving neural oscillations in the olfactory bulb (OB; Adrian, 1942). In nasal epithelium, inhaled air activates olfactory sensory neurons, which can detect both odor and mechanical stimuli (Grosmaitre, Santarelli, Tan, Luo, & Ma, 2007; Iwata, Kiyonari, & Imai, 2017). The air flowing through the nostrils can also synchronize neuronal activity and local field potentials (LFPs) in olfactory piriform cortex (Fontanini & Bower, 2005; Fontanini, Spano, & Bower, 2003). Recently, it has been observed that breathing also couples with the slow activity of brain areas that are not related to olfaction. Ito et al. (2014) showed that spikes and delta (1–4 Hz) oscillations from the somatosensory cortex (S1) phase-lock with respiration in awake mice. This cortical respiratory potential (CRP) is lost after bulbectomy. CRPs were also observed in the dentate gyrus (Lockmann, Laplagne, Leão, & Tort, 2016; Nguyen-Chi et al., 2016; Yanovsky, Ciatipis, Draguhn, Tort, & Branka, 2014), medial prefrontal (Pf), orbitofrontal cortex (Biskamp, Bartos, & Sauer, 2017; Kőszeghy, Lasztóczi, Forro, & Klausberger, 2018; Moberly et al., 2018; Zhong et al., 2017), and primary visual (V1) and motor (M1) cortex (Rojas-Líbano, Wimmer del Solar, Aguilar-Rivera, Montefusco-Siegmund, & Maldonado, 2018) of rats and mice. Other studies have shown that CRPs are also present in several regions of the human brain (Herrero, Khuvis, Yeagle, Cerf, & Mehta, 2018; Zelano et al., 2016). Respiratory modulation of local γ activity was also observed in most of the abovementioned areas (Biskamp et al., 2017; Ito et al., 2014; Manabe & Mori, 2013; Nguyen-Chi et al., 2016; Rojas-Líbano et al., 2014, 2018; Zhong et al., 2017). This "cross-frequency coupling" (CFC; Tort, Komorowski, Eichenbaum, & Kopell, 2010) has been also hypothesized to play a role in integrating distributed network activity (Tort et al., 2018a; Zhong et al., 2017).

Utilizing the cat as an animal model, the aim of the present study was to seek whether slow regional oscillatory activity phase-locks to respiration and couples with the γ activity in cortical areas during wakefulness (W) and sleep. In addition, we studied whether nasal respiration modulates inter-cortical long-range γ coherence. Our results show that during W, there is a clear interaction between nasal respiration and cat's cortical γ activity (CRP and CFC). In addition, we found that breathing modulates inter-cortical long-range γ coherence, notably entangling areas that have not been previously related neither to olfaction nor to breathing. Both CRP and γ modulation disappeared during both non-REM (NREM) and rapid eye movement (REM) sleep.

2 | MATERIALS AND METHODS

2.1 | Experimental animals

Six adult cats were used in this study. Part of these animals were also utilized in previous studies (Torterolo, Castro-Zaballa, Cavelli, Chase, & Falconi, 2016a). The animals were obtained from and determined to be in good health by the Institutional Animal Care Facility. All experimental procedures were conducted in accordance with the *Guide for the Care and Use of Laboratory Animals* (8th edition,

National Academy Press, Washington DC, 2011) and were approved by the Institutional Animal Care Commission (No: 070153-000089-17). Adequate measures were taken to minimize pain, discomfort or stress. In addition, this approach motivates the use of minimum number of animals necessary to produce reliable scientific data.

2.2 | Surgical procedures

The animals were chronically implanted with electrodes to monitor the states of sleep and W (Castro-Zaballa et al., 2013; Cavelli et al., 2017; Torterolo et al., 2015, 2016a). Prior to being anesthetized, each cat was premedicated with xylazine (2.2 mg/kg, i.m.), atropine (0.04 mg/kg, i.m.) and antibiotics (Tribrissen®, 30 mg/kg, i.m.). Anesthesia, which was initially induced with ketamine (15 mg/kg, i.m.), was maintained with a gas mixture of isoflurane in oxygen (1%–3%). The head was positioned in a stereotaxic frame, and the skull was exposed. Stainless steel screw electrodes (1 mm diameter) were placed on the surface (above the dura matter) of different cortical areas (Figure S1). In addition, bipolar electrodes were implanted in both lateral geniculate nuclei (LGN) to monitor ponto–geniculo–occipital (PGO) waves and in the orbital portion of the frontal bone to record the electro-oculogram (EOG). The electrodes were connected to a Winchester plug, which together with two plastic tubes were bonded to the skull with acrylic cement to maintain the animals in a stereotaxic head-fixed position without pain or pressure. In four animals, a craniotomy was drilled in the skull overlying the cerebellar cortex, was filled with bone wax and was subsequently used to provide access to the pons for carbachol administration (Torterolo et al., 2015, 2016a). After the animals had recovered from the preceding surgical procedures, they were adapted to the recording environment for a period of at least two weeks (Castro-Zaballa et al., 2013; Torterolo et al., 2016a).

2.3 | Experimental sessions

Sessions of 4 hours were conducted between 11 a.m. and 3 p.m. in a temperature-controlled environment (21–23°C). During these sessions (as well as during the adaptation), the animals' head was held in a stereotaxic position by four steel bars that were placed into the chronically implanted plastic tubes, while the body rested in a sleeping bag (Castro-Zaballa et al., 2013; Torterolo et al., 2016a).

The electrocorticogram (ECoG) was recorded with a monopolar (referential) configuration utilizing a common reference electrode located in the left frontal sinus (Castro-Zaballa et al., 2013; Torterolo et al., 2016a). Control experiments were made using other reference electrodes (Castro-Zaballa et al., 2013). Bipolar electromyogram (EMG) of the nuchal muscles was also monitored. The electrocardiogram, by electrodes acutely placed on the skin over the precordial region, and respiratory activity by means of a micro-effort piezo crystal infant sensor and a thermistor located in the front of the nostril were also recorded. In selected experiments, we also recorded the electrogram of the LGN and the EOG. Also, for a subset of experiments, animals were habituated to breathe through the mouth by occlusion of the nostrils for a couple of minutes for several days, to allow recording of neural activity during mouth breathing. Each cat was recorded daily for approximately 30 days to obtain complete data sets.

Bioelectric signals were amplified (×1,000), filtered (0.1–500 Hz), sampled (2048 Hz, 16 bits) and stored in a PC using the Spike 2 software (CED). Data were obtained during spontaneously occurring W, NREM and REM sleep, and during the induction of REM carbachol (REMc) or cataplexy (CA; Torterolo et al., 2015, 2016a).

2.4 | Carbachol microinjection into the nucleus pontis oralis

In order to induce REMc or CA, carbachol (0.8 μg in 0.2 μl of saline) was microinjected unilaterally for a period of 1 min into the nucleus pontis oralis (NPO) with a Hamilton syringe (Torterolo et al., 2015, 2016a). Carbachol microinjections were performed either during NREM sleep or W. Two successful carbachol microinjections (in these experiments, REMc and CA episodes were generated) were carried out for each animal (cats 3–6 in Figure S1). The animals' eyes were examined throughout the recording sessions to determine whether they were closed or open and whether the pupils were mydriatic or miotic. We also monitored the degree of relaxation of the nictitating membrane and whether the animals were able to track visual or auditory stimuli (Torterolo et al., 2015, 2016a). During CA, the ECoG resembles W, PGO waves in the LGN were not observed, the eyes were open with moderate pupillary dilatation and auditory, and visual stimuli were tracked as during natural W. In contrast, during REMc the ECoG and PGO waves in the LGN did not differ from naturally occurring REM sleep (Figure 5a; arrowheads). Additionally, the eyes were closed and the nictitating membrane was relaxed (Torterolo et al., 2015, 2016a). REMc and CA share the same muscle atonia (Figure 5a, EMG).

2.5 | Data analysis

Sleep and W were quantified in 10-s epochs applying standard classification criteria (Castro-Zaballa et al., 2013; Torterolo et al., 2016a). Then, the maximum number of non-transitional and artifact-free periods of 30 s was selected for analysis during each behavioral state (Cavelli et al., 2018). For each animal, we analyzed up to four complete recordings in order to guarantee a minimum 500-s length for each cat

and behavioral state (REM sleep is the limiting factor as it is a small percentage of the total recording time). These data were imported and analyzed offline using built-in and custom-written MATLAB codes (MathWorks). All data were previously filtered (low pass, 100 Hz) and down-sampled at 256 Hz to decrease the computational load of subsequent analyses.

Power spectrum was calculated by means of Welch's periodogram (MATLAB *pwelch* function).

Coherence spectra (Figures 1b and 5b) of electrode pairs were computed using magnitude-squared coherence (MATLAB *mscohere* function), and the Fisher z' transform was applied (z'-coherence). Both power and coherence spectrum calculations were carried out in all the data segments using 10-second Hamming windows and a frequency resolution of 0.1 Hz.

Cross-correlation function maps (CCFmap; Figures 3 and S4) were generated between respiration and the envelopes of frequencies between 20 and 100 Hz (custom-written MATLAB code). To obtain the CCFmap, several band-pass-filtered signals were generated from the raw recordings (EEGLAB *eegfilt* function [Delorme & Makeig, 2004]). We used 10 Hz bandwidth and 5 Hz steps, covering from 15 up to 105 Hz. The CCFmap was then generated by means of a raster plot of CCFs (MATLAB *xcross* function) calculated between the respiration wave and the envelopes (MATLAB *hilbert* function) of each ECoGs' filtered signal.

Phase–amplitude coupling (PAC) and modulation index (MI) (Figures 4 and 5d) were calculated using the framework previously described by Tort et al. (2010). First, the phase of the respiratory wave was extracted (*hilbert*). Second, the γ band was band-pass-filtered (30–60 Hz) and envelopes were generated (*eegfilt* and *hilbert*, respectively). Phase–amplitude plots were computed using 20° phase bins of the respiratory signal. The mean amplitude in each phase bin was normalized

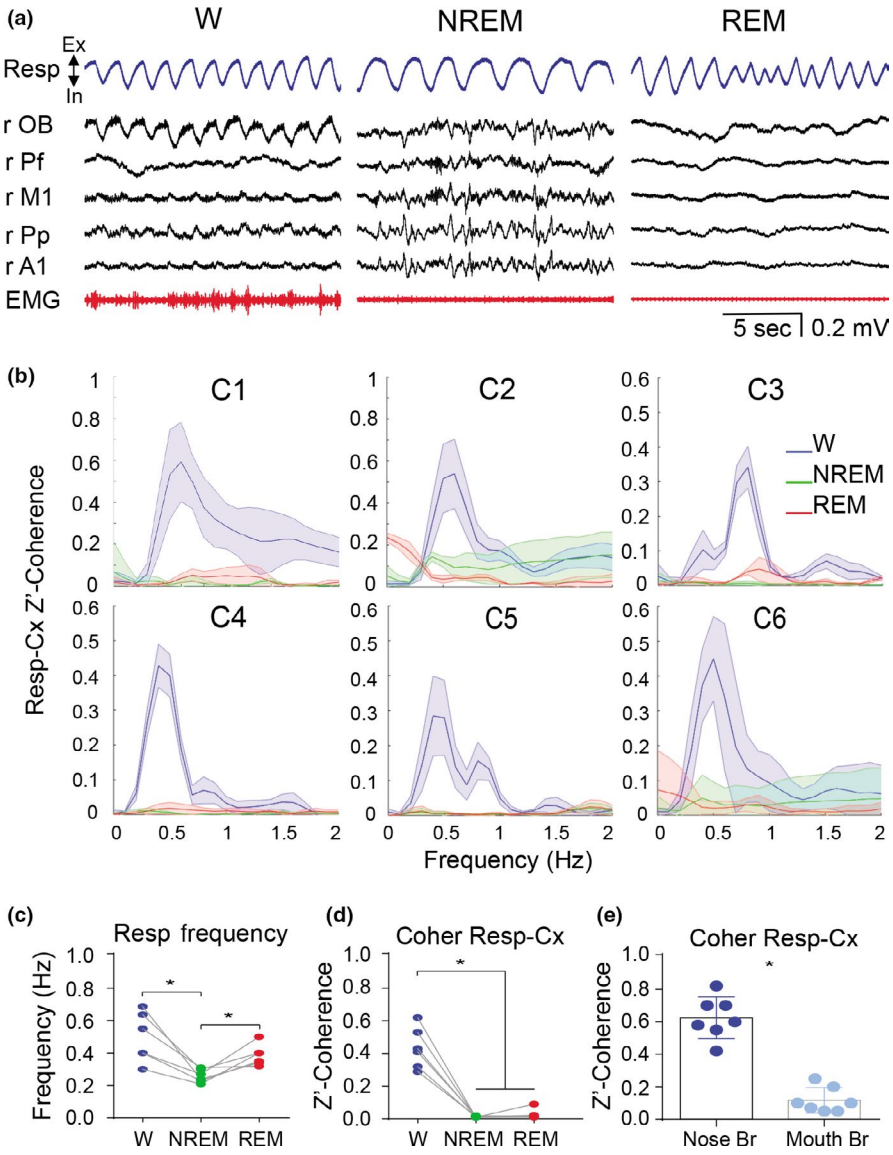

FIGURE 1 Cortical respiratory potential (CRP) in the cat's cortex during wakefulness (W) and sleep. (a) CRPs in cortical areas of a representative cat (C1) during wakefulness (W), NREM and REM sleep. Breathing is recorded by a thermistor in the nostrils (Resp, blue) simultaneously with the ECoG (black) and the electromyogram (EMG, red). (b) Z′-coherence between the respiratory waves and ECoG signals during sleep and W. The analyses were performed in each animal (C1 to C6). Each trace is the average of all the recorded channels. Shaded areas correspond to the standard deviation. (c) Respiratory frequency during W and sleep stages, which was extracted from the peak of the respiratory signal's power spectrum. (d) Z′-coherence values between the respiratory wave and the ECoG (measured at the peak of the respiratory frequency) during W, NREM and REM sleep. (e) The same analysis as in D is displayed during mouth and nose breathing for a representative animal. *$p < .05$. Br, breathing; Cx, cortex; Ex, exhalation; In, inhalation; OB, olfactory bulb; Pf, prefrontal cortex; M1, primary motor cortex; Pp, posterior parietal cortex; A1, primary auditory cortex; r, right hemisphere

by the sum across bins, so that amplitude values in each plot summed to 1. MI was calculated by the equation:

$$\mathrm{MI} = \frac{H_{\max} - H_{\mathrm{pac}}}{H_{\max}}$$

where $H_{\max}$ is the maximum entropy value (Shannon, 1948) that can be obtained from the phase–amplitude relations (uniform distribution), and H_{pac} is the entropy of the phase–amplitude relations for the original signal (Tort et al., 2010). MI = 1 means maximum PAC, while MI = 0 means absence of PAC.

γ *Coherence in function of the respiratory phase* (Figure 7a) was calculated (custom-written MATLAB code) using the phase of the respiratory signal and the coherence between pairs of the ECoG signals. After the respiratory phase extraction (*hilbert*), the pair of ECoG recordings was divided into nine parts (40° each) taking as reference the respiratory wave. Then, the coherence of each bin phase was computed using magnitude-squared coherence (*mscohere*). Thereafter, the spectral coherence was plotted as a function of the respiratory phase as a heat map.

Phase locking value (PLV) as a function of the respiratory phase (Figures 7b,c and S7) was calculated (custom-written MATLAB code) using the bin phase of the respiratory signal and the phase coherence (PLV) between each pair of the ECoG signals. After the respiratory phase bin extraction (*hilbert*), each pair of ECoG records was band-pass-filtered (10 Hz bandwidth and 5 Hz steps, covering from 15 up to 105 Hz; or 30–60 Hz) and phase-extracted (*eegfilt* and *hilbert*, respectively). Then, the ECoG phase difference was computed and the mean phase difference in the complex plane of each respiratory phase bin (20°) was calculated (PLV; Lachaux, Rodriguez, Martinerie, & Varela, 1999). PLV = 1 means that phase difference is constant through all the respiratory bins, and PLV = 0 means that phase difference changes randomly through respiratory bins. In order to discard that PLVs were an artifact produced by the lack of sinusoidality of the respiratory signal, we performed control analyses in which we assumed that the respiratory wave was sinusoidal (see Figure S7B).

R^2 *wave in function of the respiratory phase* (Figure 6) was calculated (custom-written MATLAB code) using phase bins of the respiratory signal and the waveform created from the square of the Pearson correlation coefficient (R^2 or coefficient of determination) between a pair of electrodes. After the respiratory phase bin extraction (*hilbert*), each pair of ECoG recordings was band-pass-filtered (30–60 Hz; *eegfilt*) and the coefficient of determination (R^2; MATLAB squared *corr* function) was calculated with a moving window of 0.088 second (four γ cycles) with ≈ 99% of superposition (Figure 6b). Then, the mean of the R^2 wave was calculated for each respiratory phase bin (Figure 6d). We also calculated the coherence between the γ R^2 wave and the respiratory waveform (Figure 6e).

2.6 | Statistics

Group data are expressed as mean ± standard deviation. Most of the statistical analyses were assessed by paired two-tailed *t* test (see Section 2.1 and Figure legends). The significance of the differences among behavioral states was evaluated with repeated-measures ANOVA (rmANOVA) along with the Bonferroni post hoc tests. When sphericity criteria were not accomplished (tested by Mauchly's test), the Greenhouse–Geisser correction was applied. The criterion used to reject null hypotheses was $p < .05$. For Figures 7a and S7A, a paired two-tailed *t* test was performed with a Bonferroni correction for multiple comparisons. With this correction, $p < .0001$ was considered statistically significant. The result obtained within a behavioral state was also evaluated by a permutation test (also called randomization test; see Figures 4c, 7b and S6). In this procedure, the original data were shuffled previous to perform the same analysis that was used on the raw data. This operation was repeated 250 times to obtain a distribution of randomized results. If the original result was greater than 99% or less than 1% of this distribution, we assumed that our result was statistically significant.

3 | RESULTS

3.1 | Cortical respiratory potentials are present during wakefulness but not during sleep

The ECoG from several areas of the neocortex and OB were obtained during the sleep–wake cycle of six cats (see Figure S1 for electrode location). We also simultaneously monitored the EMG and the respiratory activity.

First, we determined the presence of CRP in the ECoG and its dependence on the animal's behavioral state. Figure 1a shows the polysomnographic recording of a representative animal (C1) during W, NREM and REM sleep. During W, we observed that slow respiratory waves were accompanied by high-amplitude oscillations of similar frequency in the OB. Similar potentials of lower amplitude were also present in the neocortex (Figure 1a, top left). We detected similar CRP in the ECoG for all animals during W. During NREM sleep, although we observed the characteristic slow waves and sleep spindles, these oscillations do not seem associated with the respiratory cycle (Figure 1a, middle traces). During REM sleep, CRPs were not observed in any of the recorded areas (Figure 1a, right traces). We also found in all the animals that respiration and cortical activity were spectrally coherent during W but not during NREM and REM sleep (Figure 1b). We then calculated the respiratory rate through spectral analysis of the respiratory signal. As expected, the respiratory frequency was dependent on the behavioral state (Torterolo et al., 2015) (repeated-measures ANOVA (rmANOVA) and Bonferroni post hoc tests;

$F_{(1.144, 5.721)} = 8.158$, $p = .028$). During NREM sleep, respiration rate was lower in comparison with W and REM sleep (Figure 1c). Thereafter, we computed the average coherence levels for each animal, at the frequency of the peak of the power spectrum that corresponds to the respiratory wave (Tort et al., 2018a). Figure 1d shows that coherence values between respiratory oscillations and ECoG are large during W and decrease during sleep (rmANOVA; $F_{(1.094, 5.469)} = 66.56$, $p = .0003$). Next, we sought to determine whether these CRPs were related to the passage of air through the nostrils. As shown in Figure 1e, the coherence between respiration and ECoG that is observed during nasal respiration in W drops during mouth breathing (two-tailed t test, $p = .0001$).

Finally, circular distribution analysis of the phase differences between the OB and the neocortical electrodes exhibits phase differences other than 0° or 180° (Figure S2), suggesting that CRPs were not a result of volume conduction from the OB (Moberly et al., 2018).

3.2 | Respiration entrains cortical γ activity during wakefulness

Figure 2a shows two examples of sleep to W transitions. In both cases, CRPs are clearly associated with W but are absent during sleep. Spectrograms of Figure 2b and filtered recordings shown in Figure S3 exhibit that bursts of coupled γ band (30–50 Hz) activity are also related to W and associated with breathing.

In order to quantify the cross-frequency coupling ($CFC_{Resp\text{-}\gamma}$) between respiration and γ oscillations, we constructed cross-correlation function maps (CCFmap) between respiratory signal and ECoG amplitude envelopes in the 10–100 Hz frequency band (Cavelli et al., 2018). Figure 3 shows the CCFmaps of five neocortical areas and OB of a representative animal during W, NREM and REM sleep as well as the autocorrelation function (ACF) of the respiratory wave. We observed a clear cross-correlation between respiration and γ activity for all the recorded areas during W. On the other hand, during sleep (NREM and REM) the $CFC_{(Resp\text{-}\gamma)}$ levels are negligible. In the ACF (bottom panels in Figure 3), zero lag corresponds to the end of exhalation and beginning of inhalation. Note that γ-respiration correlation increases mainly during the exhalatory phase of the cycle. Also, the end of inhalation is accompanied by higher γ frequencies that become progressively lower as exhalation develops (see W panels in Figure 3). We found similar behavioral state-dependent changes in $CFC_{(Resp\text{-}\gamma)}$ for each recorded animal (see Figure S4). This analysis also revealed some variability among the animals regarding the frequency limits of the γ burst; in some animals, the frequency range of the bursts goes up to 60 Hz (Figure S4).

In addition, we analyzed the relationships between the phase (in degrees) of the respiratory wave and the amplitude

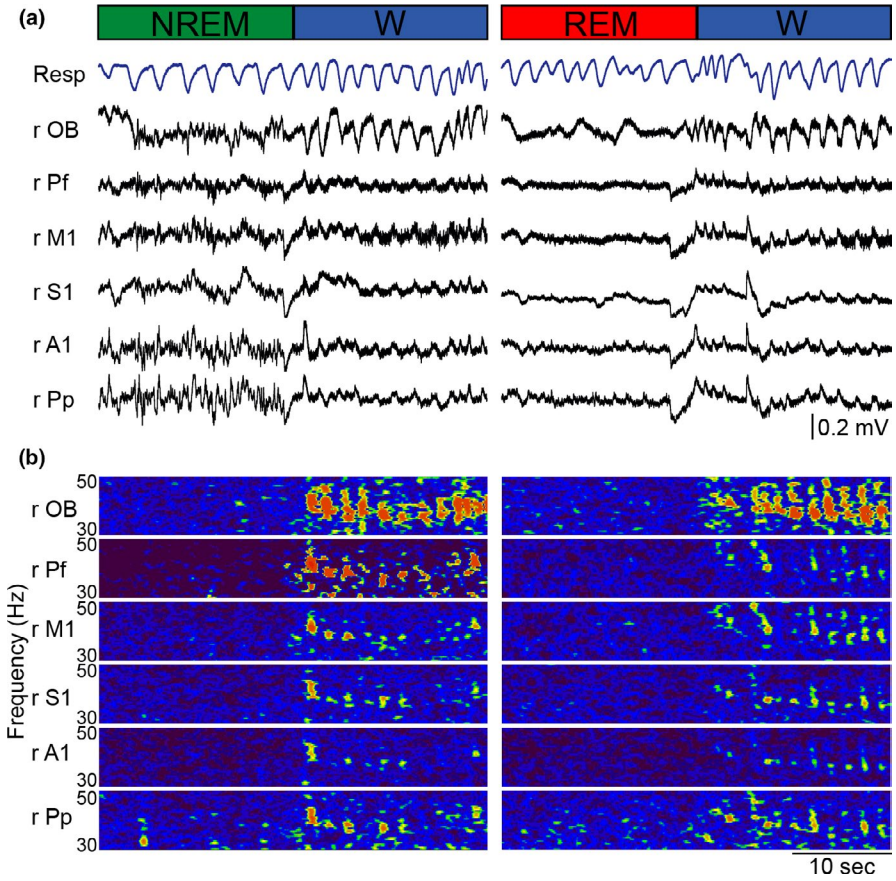

FIGURE 2 Cortical respiratory potential (CRP) during sleep/wakefulness transitions. (a) Polysomnographic recordings during the transition from NREM sleep to wakefulness (W, left), and from REM sleep to W (right). Breathing was recorded with a thermistor placed in the nostrils (Resp, blue) simultaneously with the ECoGs (black). The ECoGs are from C1 animal. (b) Spectrograms (30–50 Hz) of the recordings shown in (a). They were constructed using a 1-second sliding window (0.5 Hz resolution). OB, olfactory bulb; Pf, prefrontal cortex; M1, primary motor cortex; S1, primary somatosensory cortex A1, primary auditory cortex; Pp, posterior parietal cortex

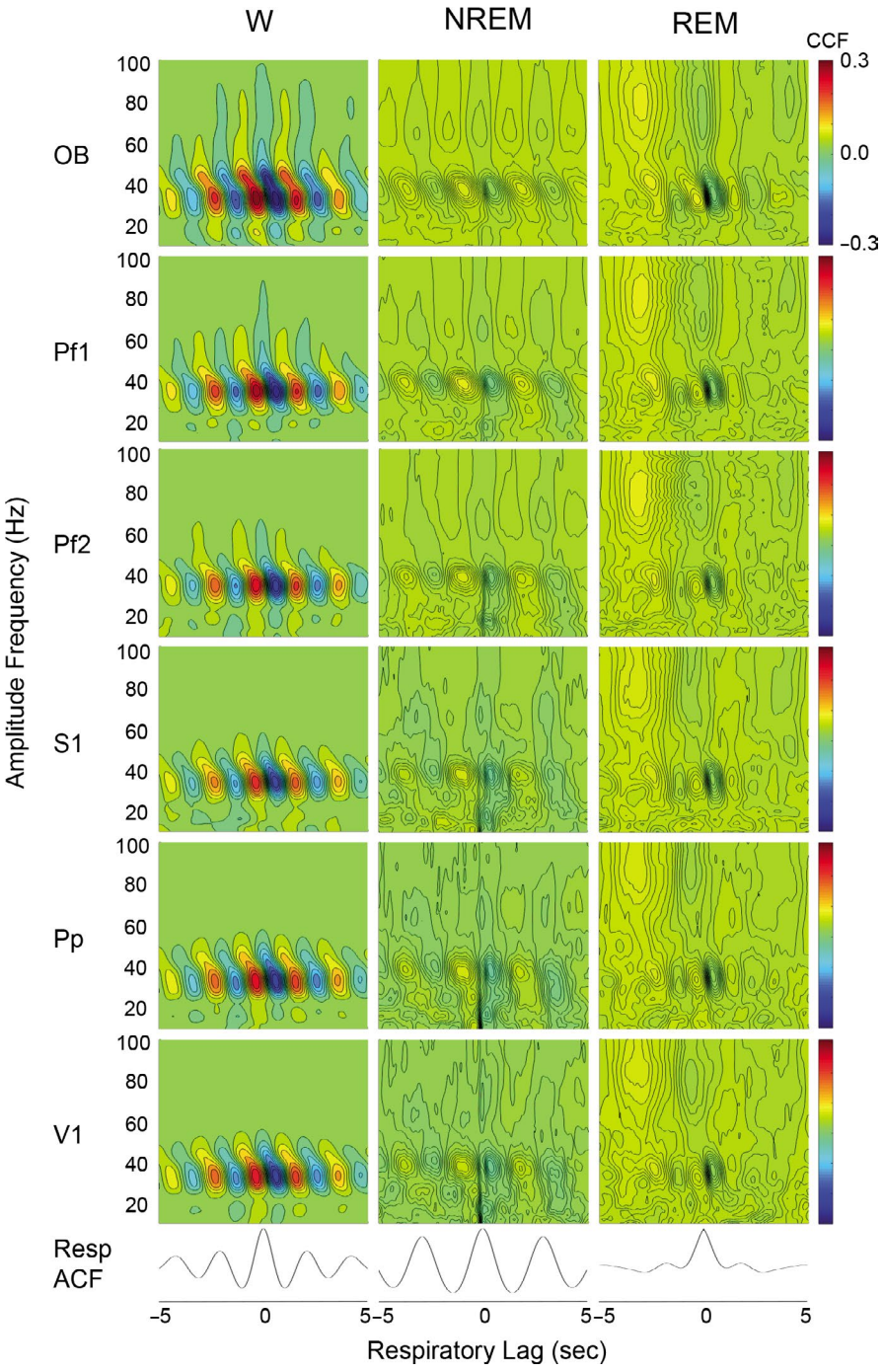

FIGURE 3 Cross-frequency coupling between cortical activity and respiration during wakefulness (W) and sleep. Color-coded panels show the cross-correlation function (CCF) between the respiratory wave and the amplitude envelope of the ECoG signals between 10 and 100 Hz (i.e., 10 Hz bandwidth with 5 Hz steps) during W, NREM and REM sleep of a representative animal (C2). The respiratory wave autocorrelation function (ACF) is also shown (bottom). Olfactory bulb (OB), anterior prefrontal cortex (Pf1), posterior prefrontal cortex (Pf2), primary somatosensory cortex (S1), posterior parietal cortex (Pp) and primary visual cortex (V1) of the right hemisphere

(envelopes) of γ activity (phase–amplitude coupling or PAC) using the modulation index (MI) designed by Tort et al. (2010). The phase–amplitude MI quantifies the deviation of the empirical phase–amplitude distribution from a uniform distribution. Figure 4a shows the average $MI_{(Resp\text{-}\gamma)}$ values of all the recorded areas for each animal ($n = 6$) during W and sleep. This analysis revealed that the highest $MI_{(Resp\text{-}\gamma)}$ values were observed during W (rmANOVA; $F_{(1.011,\ 5.057)} = 14.45$, $p = .0123$). During sleep, the values of MI not only decrease but also become similar to the distribution of randomized values (Figure S6). Furthermore, we evaluated how the $MI_{(Resp\text{-}\gamma)}$ values varied depending on the type of breathing, buccal or nasal. Figure 4b shows the MI value for all areas of a representative animal recorded during buccal and nasal breathing during W. $MI_{(Resp\text{-}\gamma)}$ was significantly higher during nasal breathing and statistically different from their own randomized values (Figure 4c).

3.3 | Respiratory cortical entrainment is also present during cataplexy (wakefulness without muscle tone)

Muscle tone is one of the main differences between W and sleep (Castro-Zaballa et al., 2013; Cavelli et al., 2017; Torterolo et al., 2015, 2016a) and is typically the main

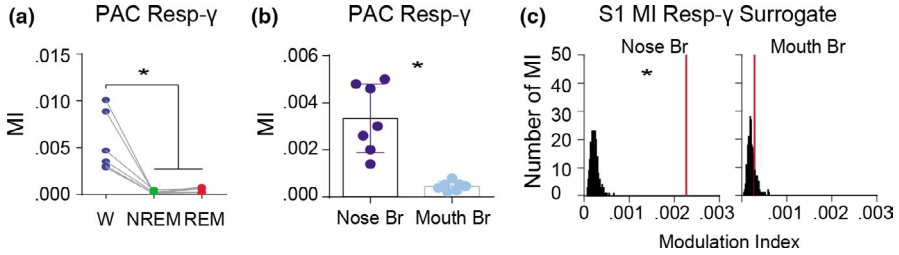

FIGURE 4 Phase–amplitude coupling (PAC) and modulation index (MI). (a) PAC between the respiratory waveform and the amplitude (envelope) of the γ cortical activity $PAC_{(Resp\text{-}\gamma)}$ for six cats, quantified by the MI during wakefulness (W), NREM and REM sleep (Tort et al., 2010). Each MI value represents the average over all cortical areas recorded for each of the six animals. (b) MI between respiratory phase and γ amplitude during mouth or nose breathing of a representative animal (C1). The values correspond to the mean ± standard deviation of the seven cortical areas recorded. (c) Histograms of randomized MI. Each graph shows the distribution of the 250 MI values obtained when we shuffled the ECoG signal (black). The red vertical line represents the MI of original result. *$p < .05$. S1, primary somatosensory cortex

artefactual signal recorded in the standard electroencephalogram, ECoG and LFPs during W (Buzsáki & Schomburg, 2015). In order to rule out the possibility that muscle activity was affecting the results, we carried out experiments in four animals where we turned off the muscular activity. The NPO is considered to exert executive control over the initiation and maintenance of REM sleep. In the cat, a single microinjection of carbachol (a cholinergic agonist) into the NPO can produce either REMc or CA for 30 min to 2 hr (Torterolo et al., 2015, 2016a). In both states, upon carbachol microinjections, we found that although the animals exhibited muscle atonia (CA and REMc) only during CA we observed CRPs (Figure 5a,b) and $CFC_{(Resp\text{-}\gamma)}$ (Figure 5c,d).

3.4 | Respiration entrains neocortical long-range γ coherence

In order to investigate whether respiratory rhythms facilitate inter-cortical functional interactions through high-frequency channels, we studied the comodulation between the respiratory waves and the cortico-cortical γ synchronization using different metrics. Figure 6a shows a polysomnographic raw recording of a representative animal during W. The same recordings but filtered for the γ band (30–60 Hz, red traces) and with the corresponding amplitudes superimposed (root-mean-square envelopes, blue traces) are exhibited in Figure 6b. This figure also shows the periodic oscillations of the coefficient of determination (R^2, gray traces) between two pairs of the previously band-pass-filtered ECoGs. It is readily observed that γ amplitude in the ECoGs and the R^2 waveform between the neocortical pairs of electrodes seem to follow the respiratory cycle (Figures 6b). Also, in Figure 6e we computed the coherence between the R^2 wave for all pairs of filtered ECoG recordings (γ: 30–60 Hz) and the respiratory signal. A large coherence at the respiratory frequency is only observed during W, where R^2 values are modulated by the respiratory phase (Figure 6d). In order to quantify this phase relationship, we analyzed the coherence of all pairs of cortices recorded as a function of the respiratory phase. Figure 7a shows the differences in coherence among behavioral states for all the animals and electrode pairs. In comparison with sleep, gamma coherence during W is modulated by the phase of respiration (Figure 7a). We obtained similar results when we analyzed the normalized phase locking value (PLV; Figure S7). In addition, Figure 7b shows that during W, in a large percentage of electrode pairs and animals gamma phase coherence was effectively modulated by the respiratory phase (randomization test). Moreover, in Figure 7c, in two representative animals we display in which pairs of electrodes the inter-cortical γ synchronization appears to be modulated by respiration during W. While the γ synchronization between neocortical areas was clearly modulated by respiration, when PLV was analyzed between neocortical areas and OB, there was not a clear phase preference (Figure 7c). Finally, while γ coherence peak and correlation are mostly present between neocortical pair of electrodes, OB–neocortical pairs do not exhibit this phenomenon (Figures 6c and 7d), despite each of the recorded areas shows similar $CFC_{(Resp\text{-}\gamma)}$ (see Figures 2b, 3, S3 and S6).

4 | DISCUSSION

Our findings provide evidence about the ability of nasal respiration to entrain neural oscillatory activity in several regions of the cat's brain. We found that nasal respiration is involved in the generation of the slow CRP and $CFC_{(Resp\text{-}\gamma)}$ in all recorded areas in a behavioral state-dependent fashion. Furthermore, we demonstrated that the phase of the respiratory cycle modulates inter-cortical γ coherence during W. This fact suggests that cross-frequency modulation between respiration and cortical γ rhythms on one side and long-range inter-cortical γ coherence on the other could be components of a single or related phenomenon.

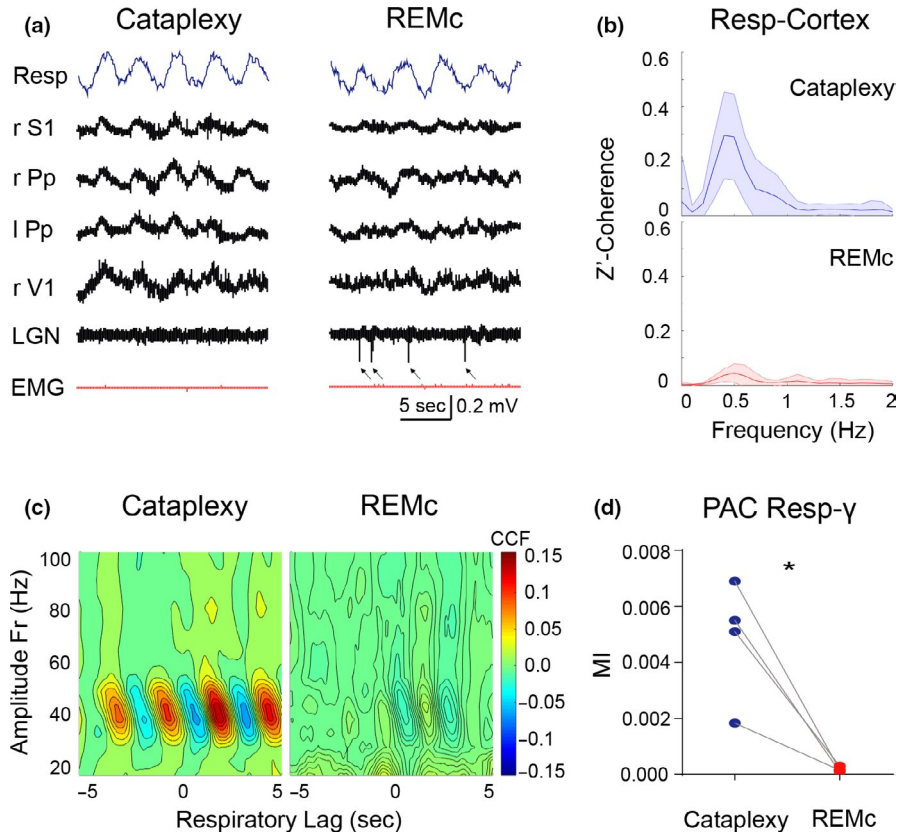

FIGURE 5 CRP and $CFC_{(Resp\text{-}\gamma)}$ were independent of the muscular tone. (a) Simultaneous polysomnographic recordings during cataplexy (CA) and REM sleep induced by carbachol (REMc). Breathing was recorded with a micro-effort piezo crystal infant sensor (Resp, blue) in simultaneous with the ECoG from the right primary sensory cortex (r S1), left and right posterior parietal cortex (l Pp and r Pp) and right primary visual cortex (r V1). Lateral geniculate nucleus (LGN) electrogram and EMG (red) are also shown. Muscle tone absence is observed in both states, but only during REMc, PGO waves were present in the LGN (arrows). (b) Z′-coherence between the respiratory wave and ECoG signals during CA and REMc. Each graph represents the mean ± standard deviation of all the cortical areas and all the animals ($n = 4$; C3–C6). (c) Mean cross-correlation function (CCF) maps during CA and REMc. Mean CCF between the respiratory waves and the amplitude envelope of the ECoG signals (between 10 and 100 Hz; 10-Hz bandwidth and 5-Hz steps) during CA and REMc are shown. The CCFmap for each condition corresponds to the mean of all the CCFmaps of every area and animal. (d) $PAC_{(Resp\text{-}\gamma)}$ during CA and REMc. Each value represents the mean modulation index (MI) value for all areas of each animal. The statistical significance between CA and REMc was evaluated with the two-tailed paired *t* test (*$p < .05$)

4.1 | Cortical respiratory potentials

The existence of CRP in the OB is well known (Adrian, 1942; Manabe & Mori, 2013; Rojas-Líbano et al., 2014). It has been shown that the slow activity of the OB faithfully follows respiration in freely behaving rats (Rojas-Líbano et al., 2014). This is possibly related to the fact that the principal neurons of the olfactory epithelium are mechanoreceptors. This implies that they do not need odorants to generate the respiratory potentials observed at the OB level (Grosmaitre et al., 2007; Iwata et al., 2017). Moreover, respiratory slow potentials can be recorded in olfactory and non-olfactory cortical areas (Fontanini et al., 2003; Ito et al., 2014; Lockmann et al., 2016; Nguyen-Chi et al., 2016; Rojas-Líbano et al., 2018; Zhong et al., 2017). In the present work, we demonstrated the presence of CRPs in the neocortex of the cat.

4.2 | Cross-frequency coupling between respiration and γ activity

CFC has been reported in electrophysiological signals such as membrane potential, LFPs, ECoG and EEG (Tort et al., 2010). A well-known CFC example occurs between the phase of the hippocampal theta rhythm (5–10 Hz) and the γ amplitude in the hippocampus and neocortex (Scheffzük et al., 2011; Sirota et al., 2008; Tort et al., 2008, 2010, 2013; Zhong et al., 2017). As mentioned in Introduction, the respiratory rhythm modulates γ activity in several areas of rodent and human brain (Biskamp et al., 2017; Herrero et al., 2018; Ito et al., 2014; Nguyen-Chi et al., 2016; Rojas-Líbano et al., 2014, 2018; Zelano et al., 2016; Zhong et al., 2017). Interestingly, recent studies in humans showed that the change from nasal to mouth breathing decreases CFC between theta and γ in

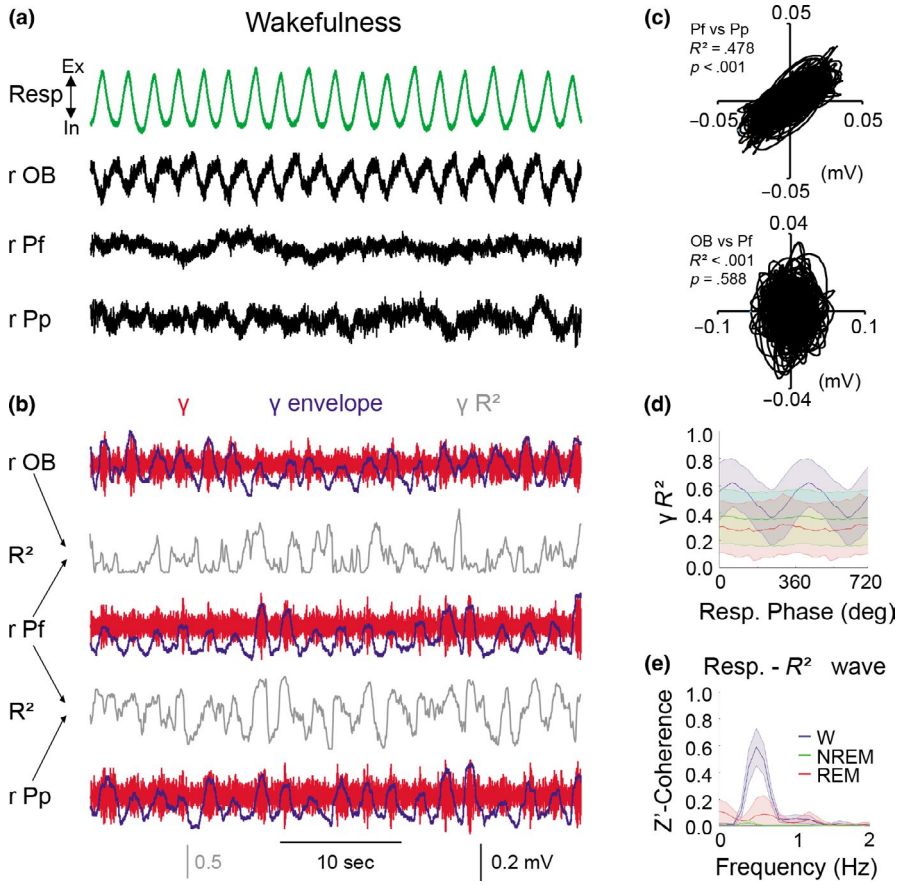

FIGURE 6 Respiratory modulation of inter-cortical γ correlation. Panel (a) shows raw ECoG recordings from different cortical areas during wakefulness (W) in simultaneous with the respiratory signal (Resp., green). (b) The respective γ band-pass-filtered ECoG signals (red traces) with their root-mean-square (RMS) envelopes (blue) superimposed are shown in panel (b). In gray, the temporal variations of the coefficient of determination (R^2 wave) processed from two ECoG channels are observed. (c) Linear correlation between pairs of previously band-pass-filtered signals for the γ band (30–60 Hz; 25 s). D. Respiratory modulation of γ R^2. The graph displays R^2 as a function of the respiratory phase. After the respiratory phase bin extraction, the average R^2 was calculated for each respiratory phase bin and behavioral state (average of all pairs and animals used). E shows the coherence between all the cortical γ R^2 waves and the respiratory waveform for all animals, electrode pairs and behavioral states

the temporal lobe and alters limbic-based behavior (Zelano et al., 2016).

In the present study, we demonstrated the existence of CFC between the phase of the respiratory wave and the amplitude of γ oscillation in the cat neocortex. It is important to note that the average frequency and limits of the γ burst differ between species (Herrero et al., 2018; Rojas-Líbano et al., 2018; Tort et al., 2018a; Zelano et al., 2016) vary according to the animal's alertness level (Rojas-Líbano et al., 2018) and to the recording site (Karalis & Sirota, 2018). In addition, we showed that this coupling remains intact during the carbachol-induced cataplexy, which strongly suggests that the muscular tone is not involved in this phenomenon.

Karalis & Sirota have recently shown in mice the coexistence of respiratory reafferent signal and the apparently corollary discharge in limbic areas (Karalis & Sirota, 2018). However, at the neocortical level this modulation of brain waves depends on air passage through the nostrils (present work) and on an intact OB (Ito et al., 2014). For this reason, it is probably that a breathing reafferent signal modulates multiple neocortical areas (Ito et al., 2014; Karalis & Sirota, 2018; Rojas-Líbano et al., 2018).

Breathing, through central autonomic integration, is also capable of regulating cardiac activity (Torterolo et al., 2015). The bottom panel in Figure S5 (tachogram, red traces) shows how respiratory sinus arrhythmia is also coupled to CRP and $CFC_{(Resp\text{-}\gamma)}$ during W. In fact, the first time we were aware of this cortical respiratory coupling was indirectly through the analysis of cat's heart rate variability (Brando, Castro-Zaballa, Falconi, Torterolo, & Migliaro, 2014; Torterolo et al., 2015). These observations are indicative of a generalized role of respiration in the coordination of bodily rhythms (Karalis & Sirota, 2018).

The existence of CRP and $CFC_{(Resp\text{-}\gamma)}$ in *Rodentia*, *Primate* genera and our results in *Carnivora* genus suggests a preserved mammal trait. Given the evolutionary importance of

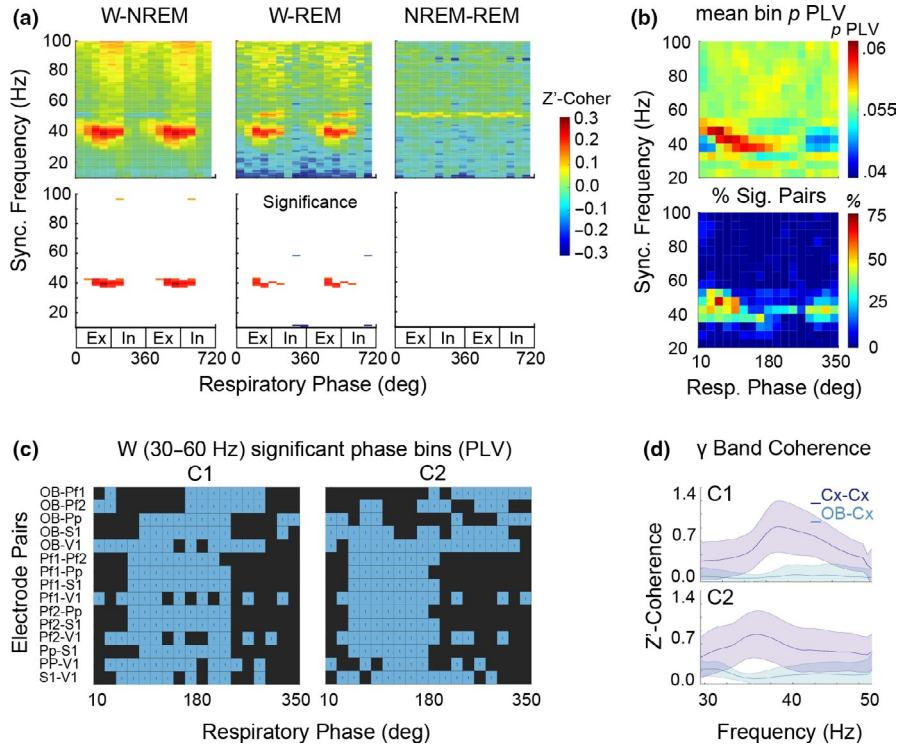

FIGURE 7 Respiratory modulation of inter-cortical γ coherence. (a) Inter-cortical Z′-coherence as a function of respiratory phase and frequency. The ECoGs' coherence was computed for each respiratory phase bin (40°, nine bins) with a frequency resolution of 0.5 Hz. Each color map at the top is the difference between two behavioral states averaged over all animals and ECoG recording pairs: W-NREM, W-REM and NREM-REM sleep. The maps at the bottom of the panel show only the statistically significant values with a $p < .0001$. (b) Inter-cortical phase locking values (PLV) as a function of the respiratory phase and frequency during wakefulness. Above, the average of the probability of obtaining a PLV for each respiratory phase bin is shown (pPLV; 20 degrees, 18 bins). Below is shown the percentage of comparisons that each phase and frequency bin was statistically different with respect to the surrogate results. Both panels are the result of all pairs and animals. (c) Shows the respiratory phase bins where the γ (30–60 Hz) PLVs were greater than 99% of the distribution of surrogate values (blue) during W. The results correspond to all pairs of electrodes of two animals (C1 and C2). Panel (d) shows the inter-cortical z'-coherence (in the γ frequency range) between the neocortical pairs (Cx–Cx) and between the OB and the neocortex pairs (OB-Cx) for the animals in panel (c). In, inhalation; Ex, exhalation

smell and the dense OB connectivity, it is highly probable to find similar phenomena in other non-mammalian vertebrates.

4.3 | Are $CFC_{(Resp-\gamma)}$ and inter-cortical γ coherence part of the same phenomenon?

Olfaction is considered an "active sensing" function where the animals produce motor actions (breathing) specifically tuned to obtain useful sensory information about their environment (Curtis & Kleinfeld, 2009; Najemnik & Geisler, 2005; Rojas-Líbano et al., 2018; Verhagen, Wesson, Netoff, White, & Wachowiak, 2007). Other examples are whisking and sniffing in rodents, electrolocation in fishes, echolocation in bats and odontocete cetaceans as well as fingers and eye movements in primates (Hofmann et al., 2013; Rojas-Líbano et al., 2018; Schroeder, Wilson, Radman, Scharfman, & Lakatos, 2010). In particular, visual exploration in primates is related to eye movement, specifically saccades and micro-saccades (Kagan & Hafed, 2013; Otero-Millan, Troncoso, Macknik, Serrano-Pedraza, & Martinez-Conde, 2008), which are highly rhythmic (Ito et al., 2013; Lowet, Roberts, Bosman, Fries, & de Weerd, 2016; Lowet et al., 2018). In visual areas, there are low-frequency oscillations phase-locked to the rhythmic saccadic movements, which exhibit a clear CFC with the γ band activity (Ito et al., 2013; Lowet et al., 2016, 2018). Something similar happens in the cortex with whisker movement in rats (Curtis & Kleinfeld, 2009; Rojas-Líbano et al., 2018) and also with nasal respiration (Ito et al., 2014; Lockmann et al., 2016; Nguyen-Chi et al., 2016; Rojas-Líbano et al., 2018; Zhong et al., 2017). Furthermore, slow waves coupled to saccadic movement are capable of modulating inter-cortical spikes and LFP γ coherence in visual areas (Lowet et al., 2016, 2018). Recently, we showed that during REM sleep hippocampal theta activity modulates the coherence of intrahemispheric high-frequency oscillations (110–160 Hz) in medial and posterior cortices of the rat (Cavelli et al., 2018). In addition, the present work demonstrates that long-range γ coherence occurs modulated by the respiratory phase, suggesting a related phenomenon. This "respiratory binding effect" is observed at the

neocortical level; however, γ coherence between OB and neocortical regions seems to be modulated differently by the respiratory activity.

Recent studies proposed that respiratory rhythms facilitated inter-regional communication via $CFC_{(Resp\text{-}\gamma)}$ (Tort et al., 2018a; Zhong et al., 2017). Other lines of research proposed that phase synchrony between areas of the brain, especially at γ frequencies, constitutes a dynamical mechanism for the control of cross-regional information flow (Fries, 2009, 2015; Womelsdorf et al., 2007). The findings of this work can potentially bring together these two theoretical frameworks in a global neocortical processing scheme; that is, high-frequency inter-regional binding is modulated by physiological rhythms such as respiration. In this way, nasal breathing could provide temporary windows of opportunity for functional integration between cortical areas.

4.4 | Cortical respiratory entrainment is not present during sleep in cat neocortex

A remarkable result in our work is that neocortical respiratory entrainment is absent during sleep. Specifically, we show that CRP, $CFC_{(Resp\text{-}\gamma)}$ and inter-cortical γ coherence are absent during NREM and REM sleep. Hence, breathing appears unable to entrain slow- and high-frequency oscillatory activity in the OB as well as in the neocortex during sleep, even when neocortical gamma power during REM sleep is similar than during quiet W (Cavelli et al., 2015, 2017). In this regard, Manabe & Mori showed that during REM and NREM sleep breathing was unable to entrain γ activity in the OB (Manabe & Mori, 2013), except for a few moments during micro-awakenings.

On the other hand, there are also studies in rodents that reported respiratory entrainment during natural sleep in some cortical structures (Jessberger, Zhong, Brankačk, & Draguhn, 2016; Karalis & Sirota, 2018; Tort et al., 2018b; Zhong et al., 2017), as well as in the sleep-like states observed during urethane anesthesia (Lockmann et al., 2016; Pagliardini, Gosgnach, & Dickson, 2013). Furthermore, it was recently shown that breathing can modulate the dynamics of limbic areas such as hippocampal ripples, and cortical UP and DOWN states, both involved in the offline processes of memory consolidation and synaptic down-selection during sleep (Heck, Kozma, & Kay, 2019; Karalis & Sirota, 2018; Liu, McAfee, & Heck, 2017; Marshall, Helgadóttir, Mölle, & Born, 2006; Tononi & Cirelli, 2019). Most of the mentioned studies in rodents use deep electrodes (LFP), unlike the present report in cats where we use ECoG. We consider that new studies are needed to find out the reasons of the differences between our and previous results.

Cognitive activity and different electrographic rhythms are generated by the activity of cortical and subcortical neurons, which are reciprocally connected. These networks are modulated by the activating or waking-promoting systems of the brainstem, hypothalamus and basal forebrain that directly or indirectly project to the thalamus and/or cortex (Cavelli et al., 2017; Torterolo, Monti, & Pandi-Perumal, 2016b). By regulating thalamocortical activities, these activating systems produce electrographic and behavioral arousal. The activating systems decrease their activity during the NREM sleep. However, while most monoaminergic systems decrease their activity during REM sleep (REM-off neurons), cholinergic neurons increase their discharge during this behavioral state (REM-on neurons), which contributes to cortical activation (Cavelli et al., 2017; Torterolo et al., 2016b). In addition, because these cholinergic neurons are active during REM sleep, they should not be critical to the generation of CRP and $CFC_{(Resp\text{-}\gamma)}$, which is absent during this state. In fact, systemic muscarinic antagonists do not block CRP and $CFC_{(Resp\text{-}\gamma)}$ in the dorsal hippocampus (Yanovsky et al., 2014) or coherent gamma activity in the cat's neocortex (Castro-Zaballa et al., 2019). More efforts must be made to unravel what neurotransmitters are involved in the generation and maintenance of this cortical respiratory entrainment.

5 | CONCLUSIONS

The results obtained in rodents, humans and the present results in felines strongly suggest that CRP and $CFC_{(Resp\text{-}\gamma)}$ are a conserved phenomenon in mammals. Extending previous findings to the cat, we confirmed the dependency on behavioral state of the cortical–respiratory coupling. We also demonstrated that nasal respiration can modulate inter-cortical coherence at γ frequency, especially between remote neocortical areas. This evidence suggests that the respiratory rhythm could facilitate inter-regional communication (Tort et al., 2018a; Zhong et al., 2017). Previously described γ synchrony between areas of the brain as a dynamical mechanism for the control of cross-regional information flow and integration process (Fries, 2009, 2015; Singer, 1999; Womelsdorf et al., 2007) could be part of a larger phenomenon, which includes respiratory modulations. In this sense, breathing and OB activity could provide constant windows of opportunity for functional integration between cortical areas. At last, the strong modulation of the electrocortical activity by the respiratory rhythms could be the foundation to understand the effect of breathing on critical functions such as memory, cognition, affection and stress responses (Heck et al., 2019; Herrero et al., 2018; Ma et al., 2017).

ACKNOWLEDGEMENTS

This study was partially supported by the "Programa de Desarrollo de Ciencias Basicas—PEDECIBA," "Proyecto I + D 2016-589, Comision Sectorial de Investigacion

Cientifica—CSIC" and "Proyecto FCE-1-2017-1-136550, Agencia Nacional de Investigación e Innovación—ANII." S. CZ. and N. V. received a postgraduate scholarship from the ANII, while M. C. received a fellowship from "Comisión de Apoyo a Postgrados—CAP." D.RL. acknowledges funding from Proyecto Fondecyt 3120185.

CONFLICT OF INTEREST

All the authors declare no conflict of interest.

DATA AVAILABILITY

For access to data and custom computer codes, contact Dr. Pablo Torterolo (ptortero@fmed.edu.uy) or Matías Cavelli (mcavelli@fmed.edu.uy).

AUTHORS CONTRIBUTIONS

Financial support: PT; Experimental design: MC, SCZ, PT; Experimental procedures: MC, SCZ, NV, PT; Analysis of the data: MC, JG, DRL, NR; Discussion and interpretation of the data: MC, PT, JG, DRL, NR, SCZ, NV; Wrote the manuscript: MC and PT. All the authors participated in critical revision of the manuscript, added important intellectual content and approved the final version.

ORCID

Matías Cavelli https://orcid.org/0000-0001-6467-5478

REFERENCES

Adrian, E. D. (1942). Olfactory reactions in the brain of the hedgehog. *Journal of Physiology*, *100*, 459–473. https://doi.org/10.1113/jphysiol.1942.sp003955

Biskamp, J., Bartos, M., & Sauer, J.-F. (2017). Organization of prefrontal network activity by respiration-related oscillations. *Scientific Reports*, *7*, 45508. https://doi.org/10.1038/srep45508

Brando, V., Castro-Zaballa, S., Falconi, A., Torterolo, P., & Migliaro, E. R. (2014). Statistical, spectral and non-linear analysis of the heart rate variability during wakefulness and sleep. *Archives Italiennes de Biologie*, *152*, 32–46.

Bressler, S. L., Coppola, R., & Nakamura, R. (1993). Episodic multiregional cortical coherence at multiple frequencies during visual task performance. *Nature*, *366*, 153–156. https://doi.org/10.1038/366153a0

Buzsáki, G., & Draguhn, A. (2004). Neuronal oscillations in cortical networks. *Science*, *304*, 1926–1929. https://doi.org/10.1126/science.1099745

Buzsáki, G., & Schomburg, E. W. (2015). What does gamma coherence tell us about inter-regional neural communication? *Nature Neuroscience*, *18*, 484–489. https://doi.org/10.1038/nn.3952

Castro-Zaballa, S., Cavelli, M., González, J., Monti, J., Falconi, A., & Torterolo, P. (2019). EEG dissociation induced by muscarinic receptor antagonists: Coherent 40 Hz oscillations in a background of slow waves and spindles. *Behavioral Brain Research*, *359*, 28–37. https://doi.org/10.1016/j.bbr.2018.10.016

Castro-Zaballa, S., Cavelli, M., Vollono, P., Chase, M. H., Falconi, A., & Torterolo, P. (2014). Inter-hemispheric coherence of neocortical gamma oscillations during sleep and wakefulness. *Neuroscience Letters*, *578*, 197–202. https://doi.org/10.1016/j.neulet.2014.06.044

Castro-Zaballa, S., Falconi, A., Chase, M. H., & Torterolo, P. (2013). Coherent neocortical 40-Hz oscillations are not present during REM sleep. *European Journal of Neuroscience*, *37*, 1330–1339. https://doi.org/10.1111/ejn.12143

Cavelli, M., Castro, S., Schwarzkopf, N., Chase, M. H., Falconi, A., & Torterolo, P. (2015). Coherent neocortical gamma oscillations decrease during REM sleep in the rat. *Behavioral Brain Research*, *281*, 318–325. https://doi.org/10.1016/j.bbr.2014.12.050

Cavelli, M., Castro-Zaballa, S., Mondino, A., Gonzalez, J., Falconi, A., & Torterolo, P. (2017). Translational Brain Rhythmicity Absence of EEG gamma coherence in a local activated cortical state: A conserved trait of REM sleep. *Translation Brain Rhythm*, *2*, 1–13.

Cavelli, M., Rojas-Líbano, D., Schwarzkopf, N., Castro-Zaballa, S., Gonzalez, J., Mondino, A., … Torterolo, P. (2018). Power and coherence of cortical high-frequency oscillations during wakefulness and sleep. *European Journal of Neuroscience*, *48*, 1–10.

Curtis, J. C., & Kleinfeld, D. (2009). Phase-to-rate transformations encode touch in cortical neurons of a scanning sensorimotor system. *Nature Neuroscience*, *12*, 492–501. https://doi.org/10.1038/nn.2283

Delorme, A., & Makeig, S. (2004). EEGLAB: An open source toolbox for analysis of single-trial EEG dynamics including independent component analysis. *Journal of Neuroscience Methods*, *134*, 9–21. https://doi.org/10.1016/j.jneumeth.2003.10.009

Engel, A. K., Fries, P., & Singer, W. (2001). Dynamic predictions: Oscillations and synchrony in top–down processing. *Nature Reviews Neuroscience*, *2*, 704–716. https://doi.org/10.1038/35094565

Fontanini, A., & Bower, J. M. (2005). Variable coupling between olfactory system activity and respiration in ketamine/xylazine anesthetized rats. *Journal of Neurophysiology*, *93*, 3573–3581. https://doi.org/10.1152/jn.01320.2004

Fontanini, A., Spano, P., & Bower, J. M. (2003). Ketamine-xylazine-induced slow (<1.5 Hz) oscillations in the rat piriform (olfactory) cortex are functionally correlated with respiration. *Journal of Neuroscience*, *23*, 7993–8001. https://doi.org/10.1523/JNEUROSCI.23-22-07993.2003

Fries, P. (2009). Neuronal Gamma-Band Synchronization as a Fundamental Process in Cortical Computation. *Annual Review of Neuroscience*, *32*, 209–224. https://doi.org/10.1146/annurev.neuro.051508.135603

Fries, P. (2015). Rhythms for cognition: Communication through coherence. *Neuron*, *88*, 220–235. https://doi.org/10.1016/j.neuron.2015.09.034

Gray, C. M., König, P., Engel, A. K., & Singer, W. (1989). Oscillatory responses in cat visual cortex exhibit inter-columnar synchronization which reflects global stimulus properties. *Nature*, *338*, 334–337. https://doi.org/10.1038/338334a0

Grosmaitre, X., Santarelli, L. C., Tan, J., Luo, M., & Ma, M. (2007). Dual functions of mammalian olfactory sensory neurons as odor detectors and mechanical sensors. *Nature Neuroscience*, *10*, 348–354. https://doi.org/10.1038/nn1856

Heck, D. H., Kozma, R., & Kay, L. M. (2019). The rhythm of memory: How breathing shapes memory function. *Journal of Neurophysiology*, *122*, 563–571. https://doi.org/10.1152/jn.00200.2019

Herrero, J. L., Khuvis, S., Yeagle, E., Cerf, M., & Mehta, A. D. (2018). Breathing above the brain stem: Volitional control and attentional modulation in humans. *Journal of Neurophysiology*, *119*, 145–159. https://doi.org/10.1152/jn.00551.2017

Hofmann, V., Sanguinetti-Scheck, J. I., Künzel, S., Geurten, B., Gómez-Sena, L., & Engelmann, J. (2013). Sensory flow shaped by active sensing: Sensorimotor strategies in electric fish. *Journal of Experimental Biology*, *216*, 2487–2500. https://doi.org/10.1242/jeb.082420

Ito, J., Maldonado, P., & Grün, S. (2013). Cross-frequency interaction of the eye-movement related LFP signals in V1 of freely viewing monkeys. *Frontiers in Systems Neuroscience*, *7*, 1.

Ito, J., Roy, S., Liu, Y., Cao, Y., Fletcher, M., Lu, L., … Heck, D. H. (2014). Whisker barrel cortex delta oscillations and gamma power in the awake mouse are linked to respiration. *Nature Communications*, *5*, 3572. https://doi.org/10.1038/ncomms4572

Iwata, R., Kiyonari, H., & Imai, T. (2017). Mechanosensory-based phase coding of odor identity in the olfactory bulb. *Neuron*, *96*, 1139–1152.e7. https://doi.org/10.1016/j.neuron.2017.11.008

Jessberger, J., Zhong, W., Brankačk, J., & Draguhn, A. (2016). Olfactory bulb field potentials and respiration in sleep-wake states of mice. *Neural Plasticity*, *2016*, 1–9. https://doi.org/10.1155/2016/4570831

John, E. R. (2002). The neurophysics of consciousness. *Brain Research Reviews*, *39*, 1–28. https://doi.org/10.1016/S0165-0173(02)00142-X

Joliot, M., Ribary, U., & Llinás, R. (1994). Human oscillatory brain activity near 40 Hz coexists with cognitive temporal binding. *Proceedings of the National Academy of Sciences of the United States of America*, *91*, 11748–11751. https://doi.org/10.1073/pnas.91.24.11748

Kagan, I., & Hafed, Z. M. (2013). Active Vision: Microsaccades direct the eye to where it matters most. *Current Biology*, *23*, R712–R714. https://doi.org/10.1016/j.cub.2013.07.038

Karalis, N., & Sirota, A. (2018). Breathing coordinates limbic network dynamics underlying memory consolidation. https://doi.org/10.2139/ssrn.3283711

Kőszeghy, Á., Lasztóczi, B., Forro, T., & Klausberger, T. (2018). Spike-timing of orbitofrontal neurons is synchronized with breathing. *Frontiers in Cellular Neuroscience*, *12*, 105. https://doi.org/10.3389/fncel.2018.00105

Lachaux, J. P., Rodriguez, E., Martinerie, J., & Varela, F. J. (1999). Measuring phase synchrony in brain signals. *Human Brain Mapping*, *8*, 194–208. https://doi.org/10.1002/(ISSN)1097-0193

Liu, Y., McAfee, S. S., & Heck, D. H. (2017). Hippocampal sharp-wave ripples in awake mice are entrained by respiration. *Scientific Reports*, *7*, 8950. https://doi.org/10.1038/s41598-017-09511-8

Lockmann, A. L. V., Laplagne, D. A., Leão, R. N., & Tort, A. B. L. (2016). A respiration-coupled rhythm in the rat hippocampus independent of theta and slow oscillations. *Journal of Neuroscience*, *36*, 5338–5352. https://doi.org/10.1523/JNEUROSCI.3452-15.2016

Lowet, E., Gips, B., Roberts, M. J., De Weerd, P., Jensen, O., & van der Eerden, J. (2018). Microsaccade-rhythmic modulation of neural synchronization and coding within and across cortical areas V1 and V2. *PLoS Biology*, *16*, e2004132. https://doi.org/10.1371/journal.pbio.2004132

Lowet, E., Roberts, M. J., Bosman, C. A., Fries, P., & de Weerd, P. (2016). Areas V1 and V2 show microsaccade-related 3-4-Hz covariation in gamma power and frequency. *European Journal of Neuroscience*, *43*, 1286–1296. https://doi.org/10.1111/ejn.13126

Ma, X., Yue, Z.-Q., Gong, Z.-Q., Zhang, H., Duan, N.-Y., Shi, Y.-T., … Li, Y.-F. (2017). The effect of diaphragmatic breathing on attention, negative affect and stress in healthy adults. *Frontiers in Psychology*, *8*, 874. https://doi.org/10.3389/fpsyg.2017.00874

Manabe, H., & Mori, K. (2013). Sniff rhythm-paced fast and slow gamma-oscillations in the olfactory bulb: Relation to tufted and mitral cells and behavioral states. *Journal of Neurophysiology*, *110*, 1593–1599. https://doi.org/10.1152/jn.00379.2013

Marshall, L., Helgadóttir, H., Mölle, M., & Born, J. (2006). Boosting slow oscillations during sleep potentiates memory. *Nature*, *444*, 610–613. https://doi.org/10.1038/nature05278

Mashour, G. A.(2006). Integrating the science of consciousness and anesthesia. *Anesthesia and Analgesia*, *103*, 975–982. https://doi.org/10.1213/01.ane.0000232442.69757.4a

Melloni, L., Molina, C., Pena, M., Torres, D., Singer, W., & Rodriguez, E. (2007). Synchronization of neural activity across cortical areas correlates with conscious perception. *Journal of Neuroscience*, *27*, 2858–2865. https://doi.org/10.1523/JNEUROSCI.4623-06.2007

Moberly, A. H., Schreck, M., Bhattarai, J. P., Zweifel, L. S., Luo, W., & Ma, M. (2018). Olfactory inputs modulate respiration-related rhythmic activity in the prefrontal cortex and freezing behavior. *Nature Communications*, *9*, 1528. https://doi.org/10.1038/s41467-018-03988-1

Najemnik, J., & Geisler, W. S. (2005). Optimal eye movement strategies in visual search. *Nature*, *434*, 387–391. https://doi.org/10.1038/nature03390

Nguyen-Chi, V., Muller, C., Wolfenstetter, T., Yanovsky, Y., Draguhn, A., Tort, A. B. L., & Branka, K. J. (2016). Hippocampal respiration-driven rhythm distinct from theta oscillations in awake mice. *Journal of Neuroscience*, *36*, 162–177. https://doi.org/10.1523/JNEUROSCI.2848-15.2016

Otero-Millan, J., Troncoso, X. G., Macknik, S. L., Serrano-Pedraza, I., & Martinez-Conde, S. (2008). Saccades and microsaccades during visual fixation, exploration, and search: Foundations for a common saccadic generator. *Journal of Visualization*, *8*, 21.1–21.18.

Pagliardini, S., Gosgnach, S., & Dickson, C. T. (2013). Spontaneous sleep-like brain state alternations and breathing characteristics in urethane anesthetized mice. *PLoS ONE*, *8*, e70411. https://doi.org/10.1371/journal.pone.0070411

Pal, D., Silverstein, B. H., Lee, H., & Mashour, G. A. (2016). Neural correlates of wakefulness, sleep, and general anesthesia. *Anesthesiology*, *125*, 929–942. https://doi.org/10.1097/ALN.0000000000001342

Rodriguez, E., George, N., Lachaux, J. P., Martinerie, J., Renault, B., & Varela, F. J. (1999). Perception's shadow: Long-distance synchronization of human brain activity. *Nature*, *397*, 430–433. https://doi.org/10.1038/17120

Rojas-Líbano, D., Frederick, D. E., Egaña, J. I., & Kay, L. M. (2014). The olfactory bulb theta rhythm follows all frequencies of diaphragmatic respiration in the freely behaving rat. *Frontiers in Behavioural Neurosciences*, *8*, 214.

Rojas-Líbano, D., Wimmer del Solar, J., Aguilar-Rivera, M., Montefusco-Siegmund, R., & Maldonado, P. E. (2018). Local cortical activity of distant brain areas can phase-lock to the olfactory bulb's respiratory rhythm in the freely behaving rat. *Journal of Neurophysiology*, *120*, 960–972. https://doi.org/10.1152/jn.00088.2018

Salinas, E., & Sejnowski, T. J. (2001). Correlated neuronal activity and the flow of neural information. *Nature Reviews Neuroscience*, *2*, 539–550. https://doi.org/10.1038/35086012

Scheffzük, C., Kukushka, V. I., Vyssotski, A. L., Draguhn, A., Tort, A. B. L., & Brankačk, J. (2011). Selective coupling between theta phase and neocortical fast gamma oscillations during REM-sleep in mice. *PLoS ONE*, *6*, e28489. https://doi.org/10.1371/journal.pone.0028489

Schroeder, C. E., Wilson, D. A., Radman, T., Scharfman, H., & Lakatos, P. (2010). Dynamics of active sensing and perceptual selection. *Current Opinion in Neurobiology*, *20*, 172–176. https://doi.org/10.1016/j.conb.2010.02.010

Shannon, C. E. (1948). A mathematical theory of communication. *Bell System Technical Journal*, *27*, 623–656. https://doi.org/10.1002/j.1538-7305.1948.tb00917.x

Singer, W. (1999). Neuronal synchrony: A versatile code for the definition of relations? Most of our knowledge about the functional organization. *Neuron*, *24*, 49–65. https://doi.org/10.1016/S0896-6273(00)80821-1

Sirota, A., Montgomery, S., Fujisawa, S., Isomura, Y., Zugaro, M., & Buzsáki, G. (2008). Entrainment of neocortical neurons and gamma oscillations by the hippocampal theta rhythm. *Neuron*, *60*, 683–697. https://doi.org/10.1016/j.neuron.2008.09.014

Tononi, G., & Cirelli, C. (2019). Sleep and synaptic down-selection. *European Journal of Neuroscience*, [Epub ahead of print]. https://doi.org/doi:10.1111/ejn.14335

Tort, A. B. L., Brankačk, J., & Draguhn, A. (2018a). Respiration-entrained brain rhythms are global but often overlooked. *Trends in Neurosciences*, *41*, 186–197. https://doi.org/10.1016/j.tins.2018.01.007

Tort, A. B. L., Komorowski, R., Eichenbaum, H., & Kopell, N. (2010). Measuring phase-amplitude coupling between neuronal oscillations of different frequencies. *Journal of Neurophysiology*, *104*, 1195–1210. https://doi.org/10.1152/jn.00106.2010

Tort, A. B. L., Kramer, M. A., Thorn, C., Gibson, D. J., Kubota, Y., Graybiel, A. M., & Kopell, N. J. (2008). Dynamic cross-frequency couplings of local field potential oscillations in rat striatum and hippocampus during performance of a T-maze task. *Proceedings of the National Academy of Sciences of the United States of America*, *105*, 20517–20522. https://doi.org/10.1073/pnas.0810524105

Tort, A. B. L., Ponsel, S., Jessberger, J., Yanovsky, Y., Brankačk, J., & Draguhn, A. (2018b). Parallel detection of theta and respiration-coupled oscillations throughout the mouse brain. *Scientific Reports*, *8*, 1–14.

Tort, A. B. L., Scheffer-Teixeira, R., Souza, B. C., Draguhn, A., & Brankačk, J. (2013). Theta-associated high-frequency oscillations (110-160 Hz) in the hippocampus and neocortex. *Progress in Neurobiology*, *100*, 1–14. https://doi.org/10.1016/j.pneurobio.2012.09.002

Torterolo, P., Castro-Zaballa, S., Cavelli, M., Chase, M. H. M. H., & Falconi, A. (2016a). Neocortical 40 Hz oscillations during carbachol-induced rapid eye movement sleep and cataplexy. *European Journal of Neuroscience*, *43*, 580–589. https://doi.org/10.1111/ejn.13151

Torterolo, P., Castro-Zaballa, S., Cavelli, M., Velasquez, N., Brando, V., Falconi, A., … Migliaro, E. R. (2015). Heart rate variability during carbachol-induced REM sleep and cataplexy. *Behavioral Brain Research*, *291*, 72–79. https://doi.org/10.1016/j.bbr.2015.05.015

Torterolo, P., Monti, J. M., & Pandi-Perumal, S. (2016b). Neuroanatomy and neuropharmacology of sleep and wakefulness. In S. R. Pandi-Perumal (Ed.), *Synopsis of sleep medicine*, 1st Edition, (506 pp). New York, NY: Apple Academic Press.

Varela, F., Lachaux, J. P., Rodriguez, E., & Martinerie, J. (2001). The brainweb: Phase synchronization and large-scale integration. *Nature Reviews Neuroscience*, *2*, 229–239. https://doi.org/10.1038/35067550

Verhagen, J. V., Wesson, D. W., Netoff, T. I., White, J. A., & Wachowiak, M. (2007). Sniffing controls an adaptive filter of sensory input to the olfactory bulb. *Nature Neuroscience*, *10*, 631–639. https://doi.org/10.1038/nn1892

Von der Malsburg, C. (1995). Binding in models of perception and brain function. *Current Opinion in Neurobiology*, *5*, 520–526. https://doi.org/10.1016/0959-4388(95)80014-X

Womelsdorf, T., Schoffelen, J.-M., Oostenveld, R., Singer, W., Desimone, R., Engel, A. K., & Fries, P. (2007). Modulation of neuronal interactions through neuronal synchronization. *Science*, *316*, 1609–1612. https://doi.org/10.1126/science.1139597

Yanovsky, Y., Ciatipis, M., Draguhn, A., Tort, A. B. L., & Branka, K. J. (2014). Slow oscillations in the mouse hippocampus entrained by nasal respiration. *Journal of Neuroscience*, *34*, 5949–5964. https://doi.org/10.1523/JNEUROSCI.5287-13.2014

Zelano, C., Jiang, H., Zhou, G., Arora, N., Schuele, S., Rosenow, J., & Gottfried, J. A. (2016). Nasal respiration entrains human limbic oscillations and modulates cognitive function. *Journal of Neuroscience*, *36*, 12448–12467. https://doi.org/10.1523/JNEUROSCI.2586-16.2016

Zhong, W., Ciatipis, M., Wolfenstetter, T., Jessberger, J., Müller, C., Ponsel, S., … Draguhn, A. (2017). Selective entrainment of gamma subbands by different slow network oscillations. *Proceedings of the National Academy of Sciences of the United States of America*, *114*, 4519–4524. https://doi.org/10.1073/pnas.1617249114

SUPPORTING INFORMATION

Additional supporting information may be found online in the Supporting Information section at the end of the article.

How to cite this article: Cavelli M, Castro-Zaballa S, Gonzalez J, et al. Nasal respiration entrains neocortical long-range gamma coherence during wakefulness. *Eur J Neurosci*. 2019;00:1–15. https://doi.org/10.1111/ejn.14560